GPS Solutions (2022) 26:39
https://doi.org/10.1007/s10291-022-01229-z

ORIGINAL ARTICLE

Improving the (re-)convergence of multi-GNSS real-time precise point positioning through regional between-satellite single-differenced ionospheric augmentation

Ahao Wang[1,2] · Yize Zhang[3] · Junping Chen[3,4] · Hu Wang[5]

Received: 23 August 2021 / Accepted: 14 December 2021

Abstract

The long (re-)convergence time seriously limits many applications of real-time precise point positioning (RTPPP) in challenging environments like urban vehicle navigation and hazards monitoring. Thus, we proposed a real-time fast-positioning model by introducing the regional between-satellite single-differenced (SD) ionospheric constraints into the undifferenced and uncombined PPP (UU-PPP). The line-of-sight ionospheric observables are extracted by the multi-GNSS (GPS + Galileo) UU-PPP method. The polynomial function with simple structure and high efficiency is applied to establish the real-time regional between-satellite SD ionospheric vertical total electron content (VTEC) model. The differential slant total electron content (dSTEC) variations retrieved from three VTEC models are validated with the between-satellite SD and epoch-differenced geometry-free combinations of dual-frequency phase observations. The average RMS values are 0.77, 0.78 and 0.47 TEC unit for the CLK93 real-time VTEC, CODE final GIM and regional between-satellite SD ionospheric VTEC model, respectively. In the positioning domain, the data of ten stations for 12 consecutive days in 2020 were used for implementing kinematic RTPPP with single-frequency (SF) and dual-frequency (DF) observations. Compared with the GPS + Galileo SF-RTPPP based on the GRoup And PHase Ionospheric Correction model, the initialization time of the SD ionospheric-constrained (SDIC) SF-RTPPP when converged to 0.2 m at the 68% confidence level can be improved from 58 to 32 min in horizontal and 72 to 49 min in vertical, and its positioning accuracy can be improved by 29.7 and 20.3% in the horizontal and vertical components, respectively. Meanwhile, the re-convergence errors of SDIC SF-RTPPP from the first epoch can be maintained at 0.15 m in three components. As to GPS + Galileo SDIC DF-RTPPP, the re-convergence time when converged to 0.1 m can be lower than 3 min in horizontal and 9 min in vertical, and the re-convergence errors at the first epoch could even be lower than 0.15 m in horizontal. Hence, the new positioning model can maintain high accuracy and improve the continuity of real-time kinematic positioning in a short time when the number of tracked satellites in the urban or canyon environment was greatly dropped due to signal blocking.

Keywords PPP with raw observations · Multi-GNSS · Real time · Ionospheric VTEC modeling · (Re-)convergence

✉ Yize Zhang
zhyize@shao.ac.cn

[1] College of Geoscience and Surveying Engineering, China University of Mining and Technology-Beijing, Beijing 100083, China

[2] Key Laboratory of Surveying and Mapping Science and Geospatial Information Technology of MNR, CASM, Beijing 100830, China

[3] Shanghai Astronomical Observatory, Chinese Academy of Sciences, Shanghai 200030, China

[4] School of Astronomy and Space Science, University of Chinese Academy of Sciences, Beijing 100049, China

[5] Chinese Academy of Surveying & Mapping, Beijing 100830, China

Introduction

Precise point positioning (PPP) proposed in the 1990s has been developed into one of the most efficient absolute positioning technologies in the global navigation satellite system (GNSS) community (Malys and Jensen 1990; Zumberge et al. 1997; Kouba and Heroux 2001). With the continuous improvement of the precise satellite orbit and clock accuracy, the millimeter- and centimeter-level positioning accuracy could be achieved in static and kinematic PPP, respectively (Guo et al. 2017). Due to the high precision of PPP technology, it has been widely used in a large number of fields such as positioning, navigation and timing (PNT)

Published online: 21 January 2022

service, natural hazard monitoring and remote sensing of the atmosphere (Petit and Jiang 2008; Wright et al. 2012). In order to further expand the application fields of PPP technology, especially in urban vehicle navigation and earthquake/tsunami early warning, real-time processing and fast convergence based on high-precision positioning have become the most important requirements of PPP users.

Thanks to the successful implementation of the Real-Time Pilot Project (RTPP) established by Real-Time Working Group (RTWG), an open-access real-time service (RTS) has been officially launched by the International GNSS Service (IGS) since April 1, 2013 (Caissy and Agrotis 2011; Hadas and Bosy 2015). Nowadays, real-time state space representative (SSR) multi-GNSS satellite orbit and clock corrections provided by several IGS analysis centers (ACs), such as CNES, BKG, GFZ and WUH, have the ability to carry out centimeter-level real-time precise point positioning (RTPPP) and support some related applications (Ahmed et al. 2016; Kazmierski et al. 2018). In regard to fast convergence, two types of real-time SSR corrections, including code and phase biases as well as ionospheric vertical total electron content (VTEC) messages, could be utilized to speed up the convergence of RTPPP. The code and phase biases are applied to the raw code and phase observations, respectively, and aimed at recovering the integer property of ambiguity in no matter what observation model (i.e., IF model, UU model) to achieve RTPPP with ambiguity resolution (AR) (Laurichesse and Blot 2016). Compared with ambiguity-float RTPPP, the average convergence time of RTPPP AR with the CNES code/phase biases could be reduced by about 30% and 44% in static and kinematic modes, respectively (Liu et al. 2020). Using STEC values derived from dual-frequency GPS observations as references, the accuracy of STEC computed with SSR VTEC products varies from 2.07 to 6.15 total electron content units (TECU) among 25 globally distributed IGS stations. With IGS post-processed global ionospheric maps (GIM) as references, the RMS of SSR VTEC varies from 0.97 to 3.01 TECU (Nie et al. 2019). Hence, the SSR VTEC products could be employed not only to real-time single-frequency (SF) positioning, but also as a priori ionospheric constraint to accelerate the convergence of RTPPP with raw observations (Wang et al. 2020a). Wang et al. (2020b) explored the contribution of SSR VTEC products to multi-GNSS SF-RTPPP solutions and reported that the convergence time of SSR-VTEC-constrained RTPPP is at least 25% faster than that of the GRoup And PHase Ionospheric Correction (GRAPHIC) RTPPP. As to the UU-PPP model, the estimation of slant ionospheric delay parameters could be strengthened by introducing a priori ionospheric variance. Many researchers suggest that regional ionospheric corrections with a better than 1 TECU accuracy are likely to achieve rapid re-convergence and instantaneous AR for GPS PPP and improve the GLONASS PPP-AR efficiency (Geng et al. 2010, 2016; Li et al. 2011). In theory, the convergence time of GNSS PPP will be further shortened as long as the external ionospheric products are sufficiently precise with better than 1–2 TECU (Li et al. 2019).

The majority of global ionosphere products like post-processed and real-time GIM are commonly generated based on the carrier-to-code leveling (CCL) method (Li et al. 2020). Although the CCL method has the advantage of being simple and effective, it is easily affected by leveling errors, including arc length, code noises and multipath effects (Ciraolo et al. 2007; Chen et al. 2018). The development of UU-PPP technology has become a powerful tool for retrieving the slant total electron content (STEC). Compared with the CCL, the observation noises and multipath errors of the STEC from the UU-PPP method could be significantly reduced by about 70% (Zhang et al. 2012). In terms of the accuracy of STEC estimates, the 0.1 and 0.3 total electron content unit (TECU) could be achieved from the UU-PPP and CCL methods after the convergence period, respectively (Liu et al. 2018). Based on this, Liu et al. (2018) established two real-time regional ionospheric VTEC models over Australia using the STEC from the UU-PPP and CCL methods, showing that the UU-PPP method has higher accuracy. However, the contribution of this regional ionospheric VTEC model proposed by Liu et al. (2018) to the RTPPP convergence has not been investigated. The gap will be filled in this paper. Since the satellite and receiver differential code biases (DCBs) are contained in the slant ionospheric observables, they need to be properly handled in the ionospheric modeling. Considering the satellite DCBs have long-term stability, they could be fixed by the IGS final DCB products, while for the receiver DCBs, they were usually estimated as constants in a short time (Sanz et al. 2017; Liu et al. 2018). In the worst case, the leveling errors of the ionospheric observables caused by time-varying receiver DCBs could reach up to 5 TECU (Ciraolo et al. 2007), thus, more attention should be paid to the processing of the receiver DCB. In this study, the between-satellite single-differenced (SD) algorithm, which is used to remove the receiver DCB effects, is introduced into the real-time regional ionospheric VTEC modeling. Besides, a fast RTPPP model based on the between-satellite SD ionospheric constraints is proposed for the first time, and the advantages of this model in positioning accuracy and (re-)convergence are presented.

This study is organized as follows. First, the function models and algorithms for the UU-PPP and regional between-satellite SD ionospheric VTEC modeling are presented. We propose a new model, which is the RTPPP based on the SD ionospheric constraints. After describing the experimental datasets and processing strategies, we assessed the quality of this regional ionospheric model over the Australian area. Further, the simulated kinematic positioning is

utilized to validate the performance of the proposed SF/DF-RTPPP model. Finally, some conclusions are given.

Methodology

The functional model of the UU-PPP needs to be introduced in order to extract high-precision line-of-sight ionospheric observables. Based on these extracted ionospheric observables, the regional between-satellite SD ionospheric VTEC model can then be established by employing the polynomial function. Finally, the new model of SD ionospheric-constrained (SDIC) RTPPP is proposed in detail.

General model of the undifferenced and uncombined PPP

The linearized equations of raw code and phase observations for GNSS can be expressed as (Liu et al. 2017):

$$\begin{cases} P_{r,i}^{s,Q} = \mathbf{u}_r^{s,Q}\cdot\mathbf{x} + c\cdot(\mathrm{d}t_r - \mathrm{d}t^{s,Q}) + Mw_r^{s,Q}\cdot \mathrm{ZWD}_r + \mu_i^Q\cdot I_{r,1}^{s,Q} + B_{r,i}^{s,Q} - B_i^{s,Q} + \varepsilon_{r,i}^{s,Q} \\ L_{r,i}^{s,Q} = \mathbf{u}_r^{s,Q}\cdot\mathbf{x} + c\cdot(\mathrm{d}t_r - \mathrm{d}t^{s,Q}) + Mw_r^{s,Q}\cdot \mathrm{ZWD}_r - \mu_i^Q\cdot I_{r,1}^{s,Q} + \lambda_i^{s,Q}\cdot N_{r,i}^{s,Q} + b_{r,i}^{s,Q} - b_i^{s,Q} + \xi_{r,i}^{s,Q} \end{cases} \tag{1}$$

where indices r, s and i denote the receiver, satellite and the frequency band, respectively; the superscript Q denotes a GNSS system of code division multiple access (CDMA) type (i.e., G for GPS, C for BDS, E for Galileo); $P_{r,i}^{s,Q}$ and $L_{r,i}^{s,Q}$ represent the observed-minus-computed (O-C) values of raw code and phase observations, respectively; $\mathbf{u}_r^{s,Q}$ is the unit vector of the component from satellite to receiver; $\mathbf{x}$ is the vector of the receiver coordinates increments with respect to a priori value; c denotes the speed of light in vacuum; dt_r and $\mathrm{dt}^{s,Q}$ represent the receiver and satellite clock offsets, respectively; ZWD_r denotes the site-specific tropospheric zenith wet delay (ZWD) and $\mathrm{Mw}_r^{s,Q}$ is the corresponding wet mapping function; $I_{r,1}^{s,Q}$ denotes the slant ionospheric delay on the frequency $f_1^{s,Q}$ and $\mu_i^Q = (\frac{f_1^{s,Q}}{f_i^{s,Q}})^2$ is the frequency-dependent multiplier factor; $N_{r,i}^{s,Q}$ denotes the integer phase ambiguity in cycles and $\lambda_i^{s,Q}$ is the wavelength of carrier phase observations; $B_{r,i}^{s,Q}$ and $B_i^{s,Q}$ represent the frequency-dependent code hardware delays for receiver and satellite, respectively; $b_{r,i}^{s,Q}$ and $b_i^{s,Q}$ denote the frequency-dependent receiver and satellite phase hardware delays, respectively; $\varepsilon_{r,i}^{s,Q}$ and $\xi_{r,i}^{s,Q}$ are the sum of measurement noises and multipath effects for code and phase observations, respectively.

Since the precise satellite clock products are calculated from the IF observations, the new satellite clock offset $\overline{\mathrm{dt}}^{s,Q}$ and receiver clock offset $\overline{\mathrm{dt}}_r$ used in the UU-PPP need to be corrected with code hardware delay as follows:

$$\begin{cases} \overline{\mathrm{dt}}^{s,Q} = \mathrm{dt}^{s,Q} + \mathrm{d}_{IF}^{s,Q}/c\,,\ \overline{\mathrm{dt}}_r = \mathrm{dt}_r + d_{r,\mathrm{IF}}/c \\ d_{\mathrm{IF}}^{s,Q} = \alpha\cdot B_1^{s,Q} + \beta\cdot B_2^{s,Q}, d_{r,\mathrm{IF}}^{s,Q} = \alpha\cdot B_{r,1}^{s,Q} + \beta\cdot B_{r,2}^{s,Q} \\ \alpha = \dfrac{(f_1^{s,Q})^2}{(f_1^{s,Q})^2 - (f_2^{s,Q})^2}, \beta = \dfrac{-(f_2^{s,Q})^2}{(f_1^{s,Q})^2 - (f_2^{s,Q})^2} \\ \mathrm{DCB}^{s,Q} = B_1^{s,Q} - B_2^{s,Q}\,,\ \mathrm{DCB}_r^{s,Q} = B_{r,1}^{s,Q} - B_{r,2}^{s,Q} \end{cases} \tag{2}$$

where $d_{\mathrm{IF}}^{s,Q}$ and $d_{r,\mathrm{IF}}^{s,Q}$ denote the ionosphere-free combination of code hardware delays for satellite and receiver, respectively; α and β represent the frequency-dependent factors, which are related to the satellite systems; $\mathrm{DCB}^{s,Q}$ and $\mathrm{DCB}_r^{s,Q}$ are frequency-dependent DCB for satellite and receiver, respectively.

Equation (2) is introduced into (1), a new equation of GNSS PPP with raw observations can be obtained as:

$$\begin{cases} P_{r,i}^{s,Q} = \mathbf{u}_r^{s,Q}\cdot\mathbf{x} + c\cdot(\mathrm{d}\bar{t}_r - \mathrm{d}\bar{t}^{s,Q}) + \mathrm{Mw}_r^{s,Q}\cdot \mathrm{ZWD}_r + \mu_i^Q\cdot I_{r,1}^{s,Q} + \mu_i^Q\cdot\beta\cdot(\mathrm{DCB}_r^{s,Q} - \mathrm{DCB}^{s,Q}) + \varepsilon_{r,i}^{s,Q} \\ L_{r,i}^{s,Q} = \mathbf{u}_r^{s,Q}\cdot\mathbf{x} + c\cdot(\mathrm{d}\bar{t}_r - \mathrm{d}\bar{t}^{s,Q}) + \mathrm{Mw}_r^{s,Q}\cdot \mathrm{ZWD}_r - \mu_i^Q\cdot I_{r,1}^{s,Q} + \lambda_i^{s,Q}\cdot N_{r,i}^{s,Q} + d_{r,\mathrm{IF}}^{s,Q} - d_{\mathrm{IF}}^{s,Q} + b_{r,i}^{s,Q} - b_i^{s,Q} + \xi_{r,i}^{s,Q} \end{cases} \tag{3}$$

where the hardware delays are linearly correlated with the ionospheric parameters and phase ambiguity parameters, thus (3) is rank-deficient, and all unknowns cannot be solved simultaneously. In order to get the full rank model, a new ionospheric parameter $\overline{I}_{r,1}^{s,Q}$ and new ambiguity parameter $\overline{N}_{r,i}^{s,Q}$ need to be re-parameterized as:

$$\begin{cases} \overline{I}_{r,1}^{s,Q} = I_{r,1}^{s,Q} + \beta\cdot(\mathrm{DCB}_r^{s,Q} - \mathrm{DCB}^{s,Q}) \\ \lambda_i^{s,Q}\cdot\overline{N}_{r,i}^{s,Q} = (\lambda_i^{s,Q}\cdot N_{r,i}^{s,Q} + b_{r,i}^{s,Q} - b_i^{s,Q}) + (d_{r,\mathrm{IF}}^{s,Q} - d_{\mathrm{IF}}^{s,Q}) + \mu_i^Q\cdot\beta\cdot(\mathrm{DCB}_r^{s,Q} - \mathrm{DCB}^{s,Q}) \end{cases} \tag{4}$$

Therefore, Eq. (3) can be rewritten as:

$$\begin{cases} P_{r,i}^{s,Q} = \mathbf{u}_r^{s,Q}\cdot\mathbf{x} + c\cdot(\mathrm{d}\bar{t}_r - \mathrm{d}\bar{t}^{s,Q}) + \mathrm{Mw}_r^{s,Q}\cdot \mathrm{ZWD}_r + \mu_i^Q\cdot\overline{I}_{r,1}^{s,Q} + \varepsilon_{r,i}^{s,Q} \\ L_{r,i}^{s,Q} = \mathbf{u}_r^{s,Q}\cdot\mathbf{x} + c\cdot(\mathrm{d}\bar{t}_r - \mathrm{d}\bar{t}^{s,Q}) + \mathrm{Mw}_r^{s,Q}\cdot \mathrm{ZWD}_r - \mu_i^Q\cdot\overline{I}_{r,1}^{s,Q} + \lambda_i^{s,Q}\cdot\overline{N}_{r,i}^{s,Q} + \xi_{r,i}^{s,Q} \end{cases} \tag{5}$$

Considering the satellite clock offset $\overline{\mathrm{dt}}^{s,Q}$ can be fixed using external precise satellite clock products, the estimable parameters vector $\mathbf{X}$ of the UU-PPP can be expressed as:

$$\mathbf{X} = [\mathbf{x}, \mathrm{d}\bar{t}_r, \mathrm{ZWD}_r, \bar{I}_{r,1}^{s,Q}, \bar{N}_{r,i}^{s,Q}]^T \tag{6}$$

where $\bar{I}_{r,1}^{s,Q}$ denotes the extracted line-of-sight ionospheric observables.

Algorithm of real-time regional between-satellite single-differenced ionospheric VTEC modeling

According to the UU-PPP model using the recovered real-time precise satellite orbits and clocks from IGS RTS, the line-of-sight ionospheric observables can be extracted by fixing the precise coordinates of the reference station in real time.

The slant ionospheric delay can be expressed as (Schaer 1999):

$$\begin{cases} I_{r,1}^{s,Q} = F \cdot \mathrm{mf}^{s,Q} \cdot \mathrm{VTEC}^{s,Q} \\ F = 40.28 \times 10^{16} \Big/ (f_1^{s,Q})^2 \\ \mathrm{mf}^{s,Q} = 1/\cos(Z^*) \\ Z^* = \arcsin(\dfrac{R_E \cdot \sin(\phi \cdot z)}{R_E + H}) \end{cases} \tag{7}$$

where F is the conversion coefficient from TECU unit to distance unit; $\mathrm{mf}^{s,Q}$ is the ionosphere mapping function; $\mathrm{VTEC}^{s,Q}$ denotes the ionospheric VTEC at ionosphere pierce point (IPP); R_E=6371 km is the mean radius of the earth and $H = 450$ km is the height of the single layer; z denotes the zenith distance at the receiver; and $\phi = 0.9782$ is the coefficient.

Combined (4) and (7), the equivalent ionospheric delay $\bar{I}_{r,1}^{s,Q}$ extracted by the UU-PPP can be expressed as:

$$\bar{I}_{r,1}^{s,Q} = F \cdot \mathrm{mf}^{s,Q} \cdot \mathrm{VTEC}^{s,Q} + (D_r^{s,Q} - D^{s,Q}) \tag{8}$$

where $D_r^{s,Q} = \beta \cdot \mathrm{DCB}_r^{s,Q}$ and $D^{s,Q} = \beta \cdot \mathrm{DCB}^{s,Q}$.

Since the satellite DCB has long-term stability, it can be accurately corrected with IGS final DCB products. Meanwhile, the computational efficiency of real-time ionospheric modeling could be improved by canceling this estimable parameter. In regard to the receiver DCB, the between-satellite SD algorithm is introduced to remove this effect as follows:

$$\begin{aligned} \Delta\bar{I}_{r,1}^{s,Q} &= \bar{I}_{r,1}^{s,Q} - \bar{I}_{r,1}^{\mathrm{ref},Q} \\ &= (F \cdot \mathrm{mf}^{s,Q} \cdot \mathrm{VTEC}^{s,Q} - F \cdot \mathrm{mf}^{\mathrm{ref},Q} \cdot \mathrm{VTEC}^{\mathrm{ref},Q}) \end{aligned} \tag{9}$$

where superscript ref denotes the reference satellite, which has the highest satellite elevation in a single GNSS system. $\Delta\bar{I}_{r,1}^{s,Q}$ is the between-satellite SD value of slant ionospheric delay.

In this study, the regional VTEC is modeled using the polynomial functions as follows:

$$\begin{cases} \mathrm{VTEC} = \sum_{i=0}^{n} \sum_{j=0}^{m} E_{\mathrm{ij}} \cdot (\varphi - \varphi_0)^i (\theta - \theta_0)^j \\ \theta - \theta_0 = \dfrac{(\gamma - \gamma_0)}{15} + (t - t_0) \end{cases} \tag{10}$$

where n and m are the order of the polynomial functions; E_{ij} is the estimable parameters of regional VTEC model; φ and φ_0 represent the geodetic latitude of IPP and modeling central point, respectively; γ and γ_0 represent the geodetic longitude of IPP and modeling central point, respectively. θ and θ_0 represent the solar hour angle at observation time t and the reference time of modeling t_0, respectively;

Combined (9) and (10), the final between-satellite SD ionospheric model can be expressed as:

$$\begin{aligned} \Delta\bar{I}_{r,1}^{s,Q} = {} & F \cdot \mathrm{mf}^{s,Q} \cdot \sum_{i=0}^{n} \sum_{j=0}^{m} E_{\mathrm{ij}} \cdot (\varphi^{s,Q} - \varphi_0)^i (\theta^{s,Q} - \theta_0)^j \\ & - F \cdot \mathrm{mf}^{\mathrm{ref},Q} \cdot \sum_{i=0}^{n} \sum_{j=0}^{m} E_{\mathrm{ij}} \cdot (\varphi^{\mathrm{ref},Q} - \varphi_0)^i (\theta^{\mathrm{ref},Q} - \theta_0)^j \end{aligned} \tag{11}$$

where n and m are usually set to 2–5 for regional ionospheric modeling at different scales.

To meet real-time processing requirements with high precision, the regional VTEC model needs to be established with the optimal order of polynomial in a short time. In our study, STECs within the latest 20 min are used in one observation window, and the reference time of modeling is defined as the middle of the window. On the basis of multiple verified tests, the order of polynomial n and m is set up to 3, and the estimated model coefficients are updated every 10 min in this research. More importantly, a reference satellite must be selected for each GNSS system in multi-GNSS ionospheric modeling.

Model of RTPPP based on the regional between-satellite single-differenced ionospheric constraints

Many contributions have proved that the UU-PPP with high-precision ionospheric constraints has better positioning performance (Shi et al. 2012; Wang et al. 2019). To maintain self-consistency with the above-mentioned regional ionospheric model, we use the between-satellite SD value of STEC $\Delta\bar{I}_{r,1}^{s,Q}$ as a virtual observation equation to enhance the undifferenced and uncombined RTPPP. For the sake of brevity, the last satellite (s-th) is set as the reference satellite, and the observation equations based on (5) can be formulated as:

$$\begin{bmatrix} \boldsymbol{P} \\ \boldsymbol{L} \\ \Delta\bar{\boldsymbol{I}} \end{bmatrix} = \begin{bmatrix} \boldsymbol{u} & \boldsymbol{e}^s & \mathrm{Mw} & \boldsymbol{E}^s & \boldsymbol{0} \\ \boldsymbol{u} & \boldsymbol{e}^s & \mathrm{Mw} & -\boldsymbol{E}^s & \boldsymbol{E}^s \\ \boldsymbol{0} & \boldsymbol{0} & \boldsymbol{0} & \boldsymbol{\Omega} & \boldsymbol{0} \end{bmatrix} \begin{bmatrix} \boldsymbol{x} \\ \mathrm{dt}_r \\ \mathrm{ZWD} \\ \bar{\boldsymbol{I}} \\ \bar{\boldsymbol{N}} \end{bmatrix} + \begin{bmatrix} \varepsilon_P \\ \varepsilon_L \\ \varepsilon_{\Delta\bar{I}} \end{bmatrix}, \boldsymbol{Q}_P, \boldsymbol{Q}_L, \mathbf{Q}_{\Delta\tilde{\mathbf{I}}} \tag{12}$$

$$\boldsymbol{\Omega} = \begin{bmatrix} 1 & \cdots & 0 & -1 \\ \vdots & \ddots & \vdots & \vdots \\ 0 & \cdots & 1 & -1 \end{bmatrix}_{(s-1)\times s} \tag{13}$$

where s denotes all tracked satellites at a particular epoch; $\boldsymbol{P} = [P^1, ..., P^s]^T$ and $\boldsymbol{L} = [L^1, ..., L^s]^T$ are the code and phase observation vectors, respectively; $\Delta\bar{\boldsymbol{I}} = [\Delta\bar{I}^1, ..., \Delta\bar{I}^{s-1}]^T$ is the vector of the between-satellite SD ionospheric delays; $\boldsymbol{e}^s$ is the s-column vector with all elements being 1; $\boldsymbol{E}^s$ is the identity matrix of dimension s and $\boldsymbol{0}$ is the vector with all elements being 0; $\bar{\boldsymbol{I}} = [\bar{I}^1, ..., \bar{I}^s]^T$ and $\bar{\boldsymbol{N}} = [\bar{N}^1, ..., \bar{N}^s]^T$ are the vectors of the slant ionospheric delays and phase ambiguities, respectively; $\boldsymbol{Q}_P$ and $\boldsymbol{Q}_L$ denote the stochastic model of O-C values for code and phase observations; $\boldsymbol{Q}_{\Delta\tilde{I}}$ denotes the stochastic model of virtual ionospheric observations;$\boldsymbol{\Omega}$ denotes the coefficient matrix of a priori between-satellite SD ionospheric delays, and assuming that the last satellite (s-th) is set up to the reference satellite.

Noted that the positioning performance of the ionospheric-constrained PPP is greatly affected by the weight of virtual ionospheric observations, based on multiple test verifications, we define the variance of the between-satellite SD ionospheric parameters as:

$$\sigma^2_{\mathrm{ion}} = \left(a^2 + \frac{a^2}{\sin^2(\mathrm{Ele})}\right) \cdot b \tag{14}$$

where Ele denotes the satellite elevation. According to the different types of GNSS observations (GPS/GLONASS/BDS/Galileo), a and b can be set as 0.2–0.5 and 20–50, respectively. In this study, $a = 0.2$ and $b = 30$ are suitable for GPS and Galileo PPP based on the between-satellite SD ionospheric constraints.

Experimental data and processing strategy

To verify the effectiveness of the proposed positioning model, the data sets need to be described before experiments, and two processing strategies of regional ionospheric modeling and SF/DF-RTPPP are summarized in this section.

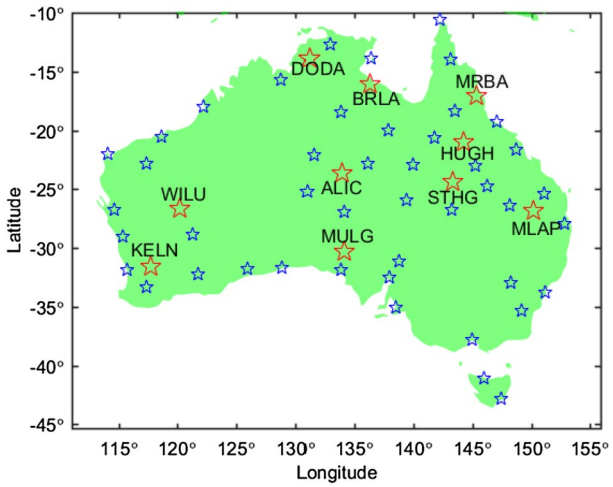

Fig. 1 Distribution of the selected 55 APREF stations (45 blue and ten red stations)

Datasets

Multi-GNSS observations sampled at 30 s were collected from 55 stations in the Asia–Pacific Reference Frame (APREF) network, which covered a 12-day period of DoY (Day of Year) 190–201 in 2020. These selected stations (shown in Fig. 1) are well-distributed across the Australian area and have great coverage for the IPPs. Note that 45 blue stations are used for the regional ionospheric VTEC modeling, and ten red stations are used to evaluate the performance of RTPPP with ionospheric augmentation.

Processing strategies

The Net_Diff software (https://github.com/YizeZhang/Net_Diff, Zhang et al. 2020) developed by Shanghai Astronomical Observatory, Chinese Academy of Sciences was used to extract STECs using the UU-PPP method, establish the regional between-satellite SD ionospheric VTEC model and carry out multi-GNSS RTPPP with ionospheric augmentation. Note that the SSR corrections provided by CNES via CLK93 mountpoint and broadcast ephemeris were utilized to recover the real-time precise satellite orbits and clocks (Kazmierski et al. 2020). Since the GPS and Galileo observations are used in the experiments, the inter-system biases (ISBs) need to be estimated as random-walk noise in the multi-GNSS combined solutions (Zhou et al. 2019). Besides, the precise coordinates of all stations are obtained from the APR daily solutions in solution-independent exchange (SINEX) format. The adopted models and processing strategies are given in Table 1.

Table 1 Adopted models and processing strategies in the experiments

Item	Models/strategies
I: RTPPP processing	
Frequency selection	GPS: L1/L2; Galileo: E1/E5a
Elevation cutoff angle	10°
Satellite orbits and clocks	Broadcast ephemeris + CNES CLK93 corrections
Estimator	Kalman filter
Weighing strategies	Elevation-dependent weighing model; a priori precision of the GPS/Galileo code and phase observations is set to 0.3/0.3 and 0.003/0.01 m, respectively (Hadas et al. 2019)
Satellite antenna correction	PCO (phase center offset)/PCV (phase center variation) values for GPS and Galileo from igs14.atx are used
Receiver antenna correction	PCO /PCV values for GPS from igs14.atx are used; Corrections for Galileo are assumed the same with GPS
DCB correction	Corrected with IGS daily DCB products
Tidal effects	Considering solid tides, ocean loading tides and polar tides
Other corrections	Considering phase windup, relativistic and earth rotation effects
Station coordinates	Static: estimated as constants Kinematic: estimated as white noise
Tropospheric delay	Modified (GPT2w + SAAS + VMF) for the dry part and estimated for the wet part as random-walk noise
Ionospheric delay	Estimated as random-walk noise
Receiver clock	Estimated as white noise
Receiver ISB	Set up for Galileo and estimated as random-walk noise
Phase ambiguities	Estimated as float constants if no cycle slip occurs
II: Regional between-satellite single-differenced ionospheric VTEC modeling	
Slant ionospheric delays	Retrieved from GPS + Galileo DF-RTPPP with raw observations
Function for VTEC modeling	Polynomial function (3 × 3 orders, 10-min interval)
Satellite DCB	Fixed to IGS daily DCB values
Stochastic model	Variance information from RTPPP with raw observations is used
Estimator	Sequential least-square method

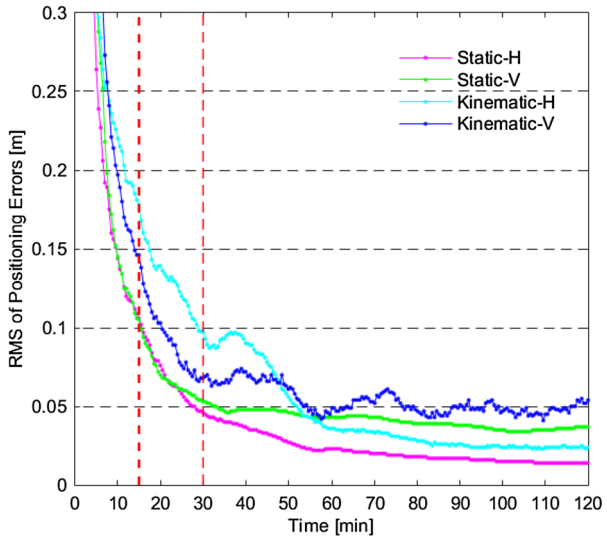

Fig.2 RMS of positioning errors during the first 2 h for all selected stations (DoY 190–201, 2020)

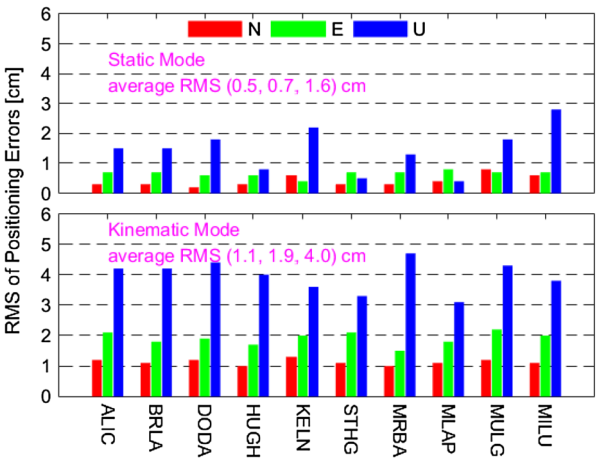

Fig. 3 RMS of positioning errors for different stations in static and kinematic modes (DoY 190–201, 2020)

Quality assessment of real-time regional between-satellite single-differenced ionospheric VTEC model

Considering that the accuracy of the ionospheric model is highly related to RTPPP performance, it is necessary to evaluate the quality of the proposed real-time regional between-satellite SD ionospheric VTEC model from different aspects before positioning verification.

Performance of the undifferenced and uncombined RTPPP

Ten red stations distributed in different areas shown in Fig. 1 were selected for real-time positioning experiments. Static and kinematic modes of the undifferenced and uncombined RTPPP using GPS and Galileo observations from DoY 190–201 in 2020 were carried out. Figure 2 shows the time series of the RMS positioning errors during the first 2 h for all stations in the whole test period. Obviously, the convergence time of static RTPPP is much better than that of kinematic RTPPP at both horizontal and vertical components. In regard to static mode, the convergence time for the RMS positioning errors of lower than 0.1 m is about 15 min, while for kinematic mode, this time could be increased to 30 and 20 min at the horizontal and vertical components, respectively. All positioning errors could be stabilized within 5 cm after 2 h convergence.

The RMS of positioning errors after 2-h convergence for different stations is given in Fig. 3. In kinematic mode, average RMS values are 1.1, 1.9 and 4.0 cm in the north (N), east (E) and up (U) components, respectively. While for static mode, the RMS values of all stations are within 1 cm in horizontal, and most of them are lower than 2 cm in vertical. Average RMS values in static mode are 0.5, 0.7 and 1.6 cm for N, E, and U components. This evaluation proved that the UU-PPP using CLK93 products has good positioning performance and makes the real-time extraction of the line-of-sight ionospheric observables possible. Note that the station coordinates are fixed to the APR daily solutions instead of estimated as constants in the ionospheric extraction from the UU-PPP method.

Real-time regional between-satellite single-differenced ionospheric VTEC modeling over the Australian area

Fifty-five stations (45 blue and ten red stations as shown in Fig. 1) collected from the APREF network during the period of DoY 190–201 in 2020 were used to model the between-satellite SD ionospheric VTECs over Australia in real time. In the test period, the ionosphere conditions and solar activity are relatively calm since most of the geomagnetic Kp index is less than 2 and the radio flux index F10.7 is no more than 70 sfu (http://isgi.unistra.fr/data_download.php). To validate the performance of the proposed real-time ionospheric model, the internal and external accord accuracy of the SD slant ionospheric delays at IPPs are employed as two indicators in this experiment. Firstly, the slant ionospheric delays are extracted by the UU-PPP method, and the satellite with the highest elevation in a single system is selected as the reference satellite, then the between-satellite SD algorithm is used to generate the SD slant ionospheric delays for ten red stations as the references. The internal accord accuracy is the difference between the referenced SD slant ionospheric delays and the modeled values are retrieved from the regional ionospheric VTEC model established by 55 stations (including ten red stations). As to the external accord accuracy, the only difference is that 45 blue stations are utilized to establish the regional ionospheric VTEC model.

Figure 4 shows the time series of the SD slant ionospheric delay errors of GPS and Galileo satellites for four red stations during the 2–24 h with the sample interval of 30 s on DoY 201, 2020. These sample stations are distributed in different regions of Australia. Since the first 2 h of the UU-PPP belongs to the convergence period, the extracted slant ionospheric delays after GPS time (GPST) 02:00:00 are used for regional ionospheric modeling in this experiment. As expected, the internal accord accuracy of the SD slant ionospheric delays is much better than external accord accuracy. The internal accord accuracy of GPS and Galileo satellites have similar performance, and their errors keep within 0.1 m. As to external accord accuracy, the SD slant ionospheric delay errors of all stations are within 0.2 m, and most of these errors vary from -0.1 to 0.1 m. The external accord accuracy of the MULG and WILU stations is slightly worse than that of other stations; the main reason is that the ionospheric properties of these areas cannot be well-described by the polynomial function model using the relatively sparse network. However, such reduction in ionospheric external accord accuracy with several centimeters for minority satellite at one epoch has little effect on the between-satellite SD ionospheric modeling.

Figure 5 gives the RMS of the SD slant ionospheric delay errors of GPS and Galileo satellites for ten red stations during a 12-day test period. As we can see, the RMS of internal accord accuracy for GPS and Galileo satellites is about 2 cm, while for the external accord accuracy, its RMS values are between 5 and 8 cm. The average RMS values of internal accord accuracy for GPS and Galileo satellites are 2.1 cm and 2.0 cm, respectively. As to the external accord accuracy, the average RMS values of GPS and Galileo satellites are 6.7 cm and 7.1 cm, respectively.

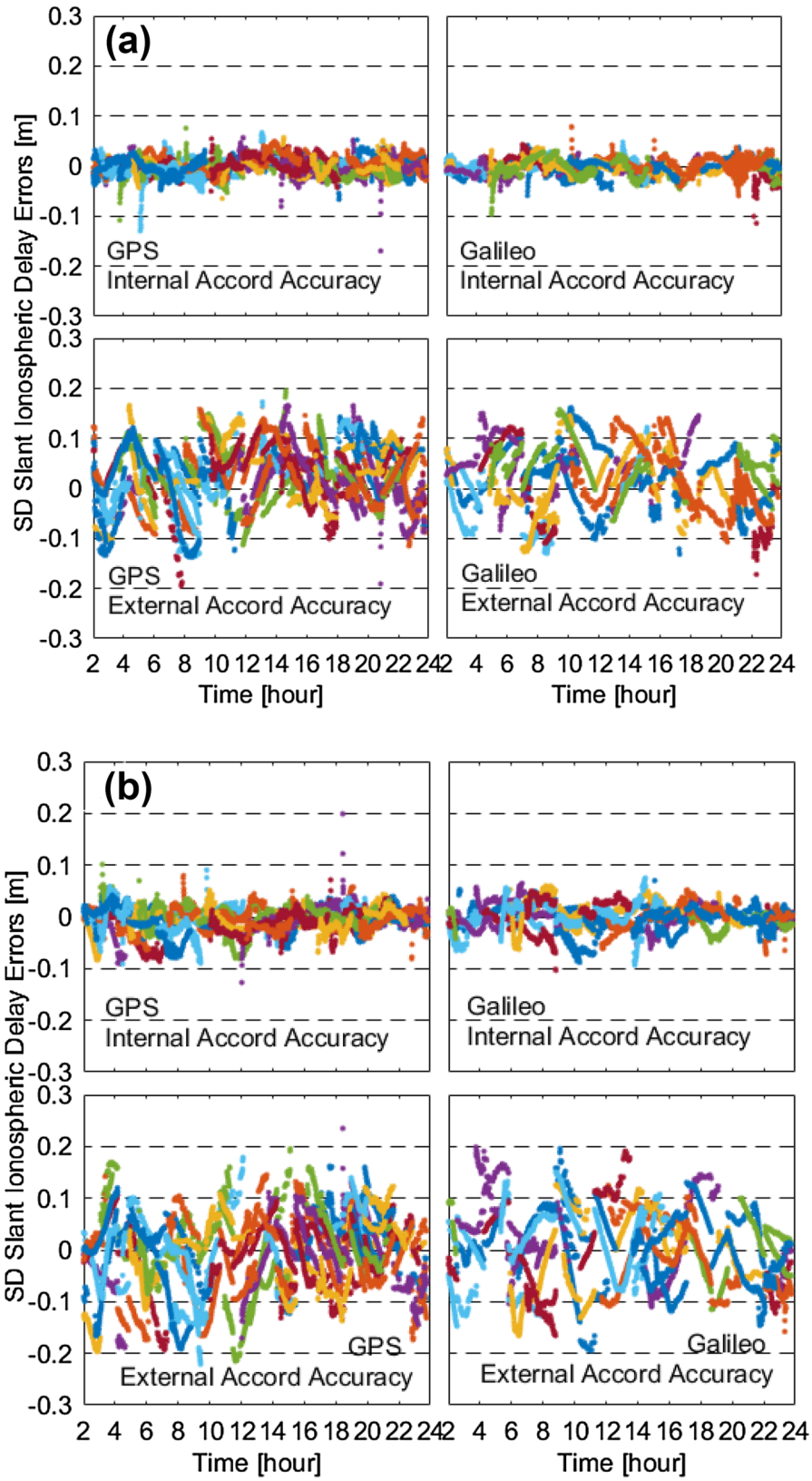

Fig. 4 Time series of the SD slant ionospheric delay errors of GPS and Galileo satellites (different colors stand for different satellites) for **a** BRLA, **b** MULG, **c** STHG and **d** WILU stations (DoY 201, 2020)

Fig. 4 (continued)

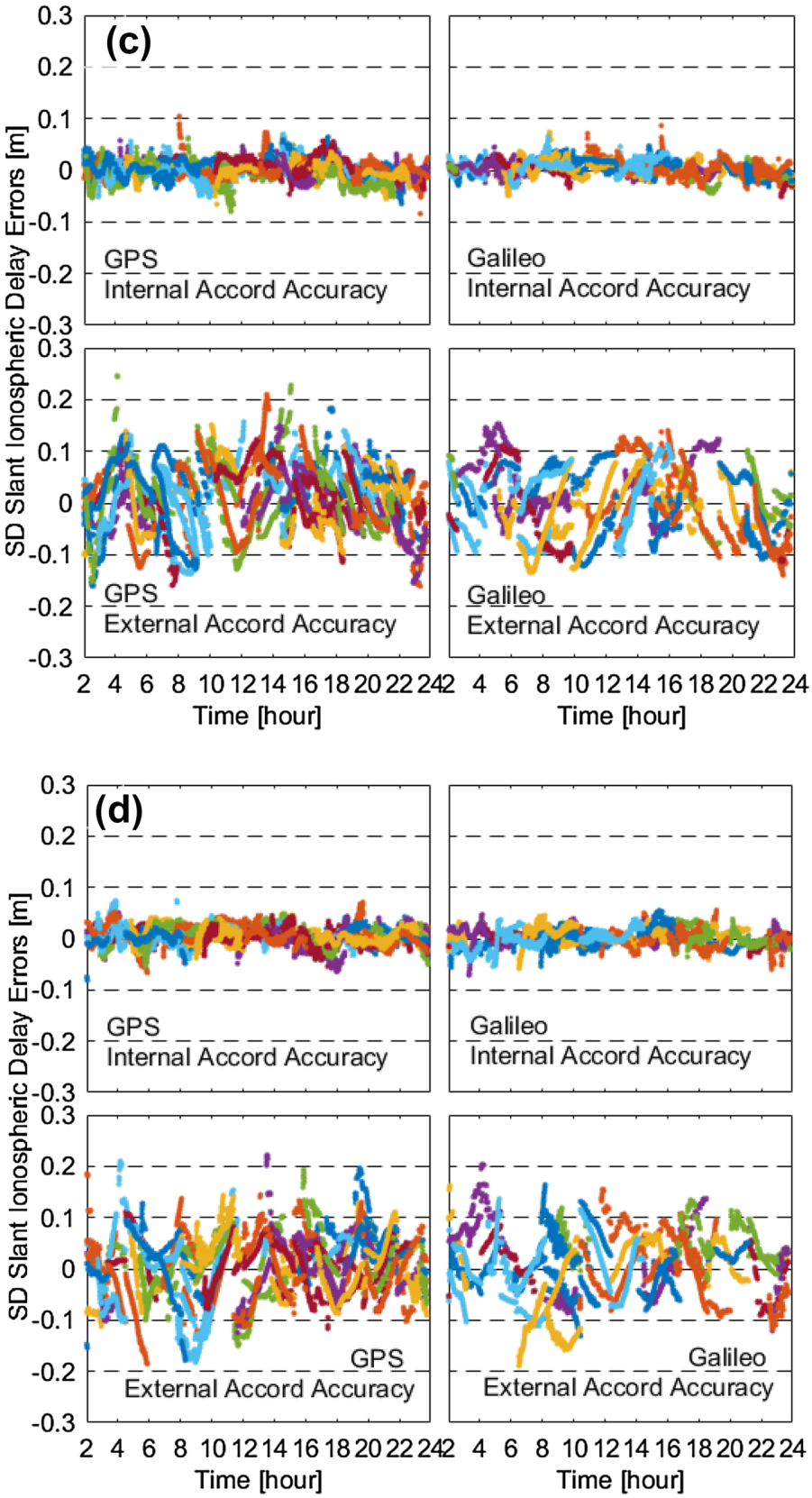

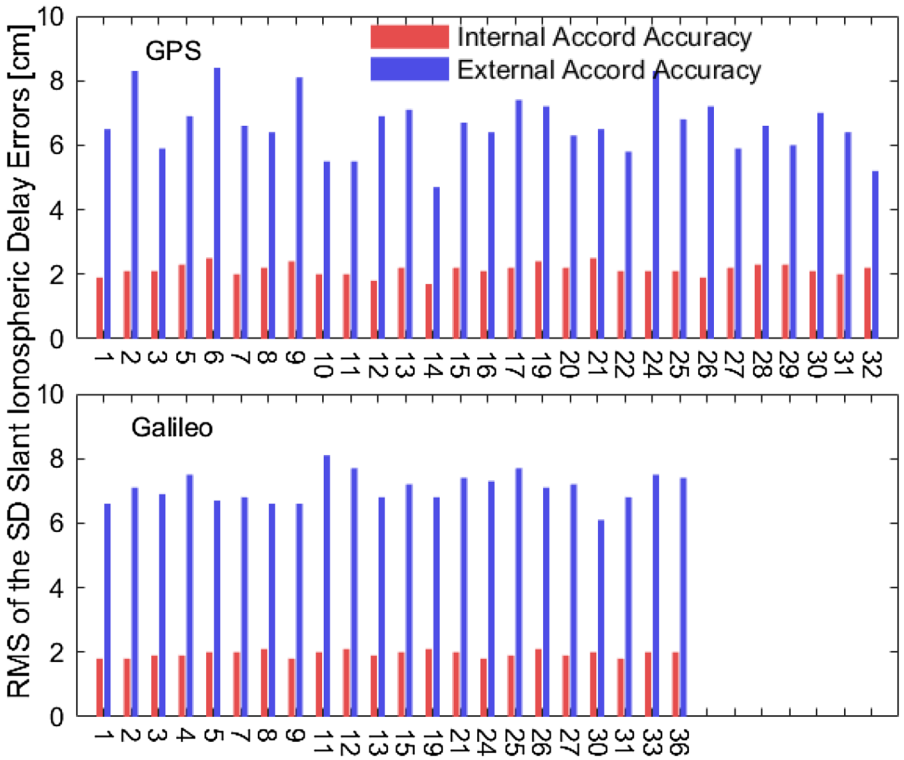

Fig. 5 RMS of the SD slant ionospheric delay errors of GPS and Galileo satellites for ten red stations (DoY 190–201, 2020)

In order to validate the excellent performance of the proposed regional ionospheric model, CNES CLK93 real-time ionospheric products (CLK93-VTEC) and CODE final GIM products (CODE-GIM) are used for comparison. In this assessment, the true STEC variations with millimeter level accuracy are first calculated from the epoch-differenced geometry-free (GF) combinations of carrier phase observations in continuous arcs, and then differential STEC (dSTEC) variations can be determined through the between-satellite SD algorithm (Liu et al. 2018). These true dSTEC variations are considered as the referenced values to validate the performances of different ionospheric VTEC models. During the processing of the modeled dSTEC variations retrieved from different ionospheric models, first, the dSTEC can be determined as the difference between the slant ionospheric delays of one satellite and that of satellite with the highest elevation in a single GNSS system. Second, the epoch-differenced algorithm is introduced into dSTEC to generate dSTEC variations (Feltens et al. 2011). Note that all test data in this section are provided at 5 min intervals and are limited to an elevation cutoff of 10 degrees. In brief, the dSTEC variation differences are defined as the difference between the modeled dSTEC variations and the referenced dSTEC variations.

Figure 6 shows the dSTEC variation differences of GPS and Galileo satellites for four red stations in DoY 201, 2020, for CLK93-VTEC model, CODE-GIM model and the proposed SD ionospheric VTEC model (SD-VTEC),

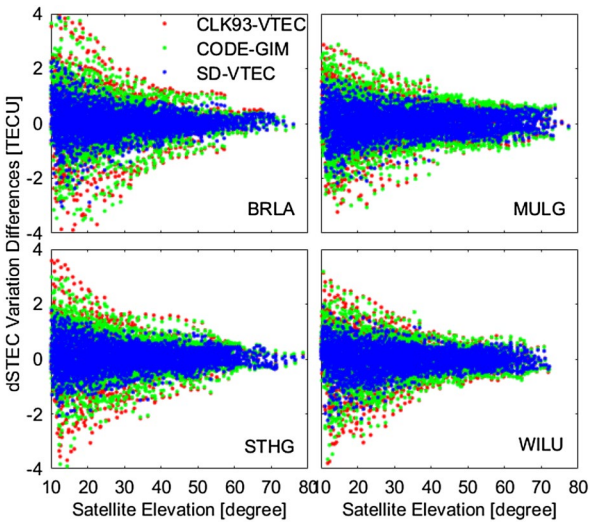

Fig. 6 dSTEC variation differences of GPS and Galileo satellites for different stations (DoY 201, 2020)

respectively. It can be seen that the dSTEC variation differences of different ionospheric VTEC models exhibit approximately normal distribution and are highly dependent on the satellite elevation, which errors could be increased with the decrease in satellite elevation. Apparently, the dSTEC variation differences of SD-VTEC model are much better than that of other ionospheric VTEC models, especially in the low satellite elevation conditions. The dSTEC

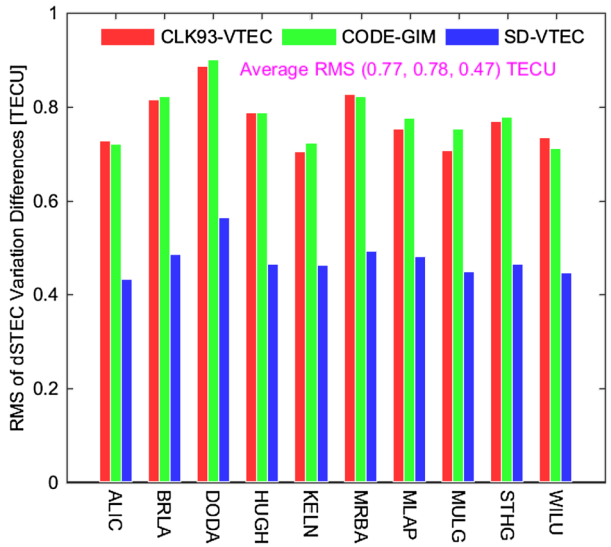

Fig. 7 RMS of dSTEC variation differences with different ionospheric VTEC models for ten red stations (DoY 190–201, 2020)

variation differences with 10–15 degrees of satellite elevation for CLK93-VTEC and CODE-GIM models may be up to 4 TECU, while for SD-VTEC model, their values can be lower than 2 TECU.

Figure 7 gives the RMS of dSTEC variation differences with three ionospheric VTEC models for all red stations in the whole test period. From the statistical results, the dSTEC variation differences of CLK93-VTEC and CODE-GIM models have the similar performance, and their RMS values for all stations are much larger than that of SD-VTEC model. Average RMS values of dSTEC variation differences are 0.77, 0.78 and 0.47 TECU for CLK93-VTEC model, CODE-GIM model and SD-VTEC model, respectively. Hence, the regional ionospheric properties can be described more precisely by the proposed SD ionospheric VTEC model. One reason is that the line-of-sight ionospheric observables are extracted by the UU-PPP method rather than CCL method, another is that dense reference stations are used to establish this regional ionospheric model.

Real-time positioning results and discussions

Based on the above-mentioned ionospheric quality assessment, the influences of the regional SD ionospheric model on the kinematic RTPPP using DF and SF observations are investigated in this section. In addition, some interesting findings are presented and discussed.

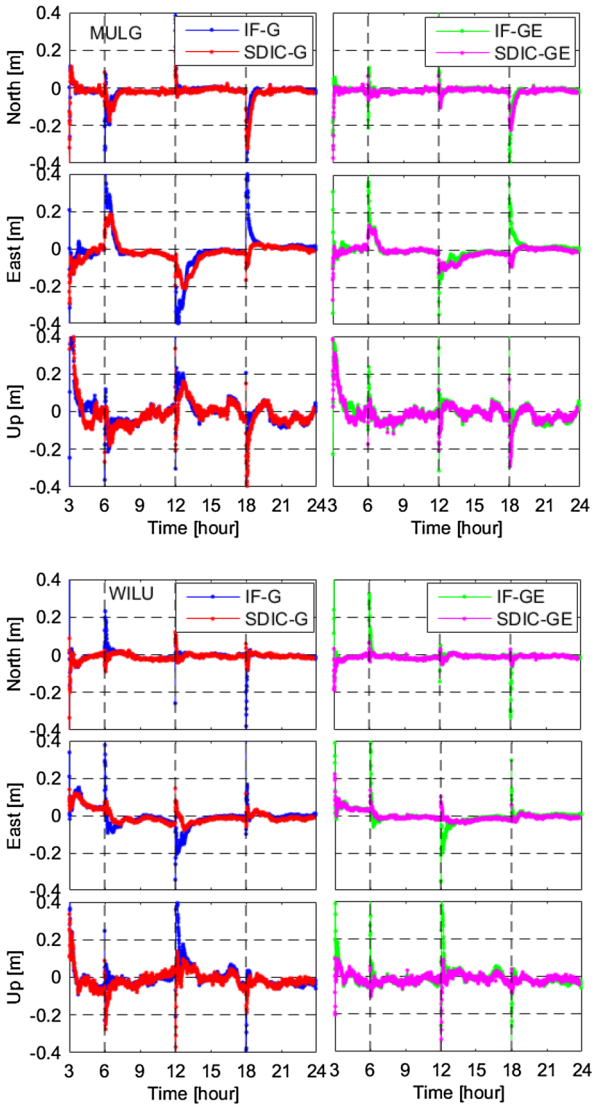

Fig. 8 Kinematic positioning errors of dual-frequency RTPPP with different solutions for MULG and WILU stations (DoY 193, 2020). The abbreviation G and E denote GPS and Galileo, respectively

Dual-frequency RTPPP

To evaluate the performance of DF-RTPPP based on the SD ionospheric constraints, the traditional DF-RTPPP using IF combinations is used as the reference for the same data processing. Figure 8 depicts the kinematic positioning errors of DF-RTPPP with two models for different stations during the 3–24 h on DoY 193 in 2020. The items of IF and SDIC in the figure denote the ionospheric-free RTPPP and the regional between-satellite SD ionospheric-constrained RTPPP, respectively. Since the proposed ionospheric model was established after GPST 02:00:00, RTPPP with the stable SD ionospheric constraints was carried out after GPST 03:00:00 in this experiment. Noted that the simulated signal

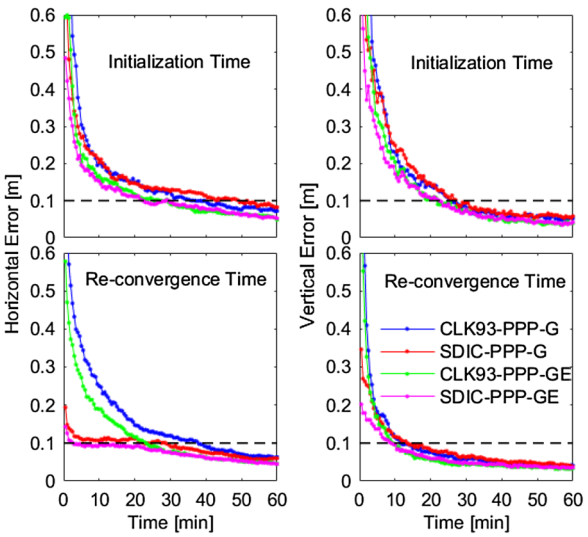

Fig.9 Convergence performance of kinematic dual-frequency RTPPP with different solutions at the 68% confidence level (10 red stations, DoY 190–201, 2020)

interruptions are introduced into GPST 06:00:00, 12:00:00 and 18:00:00 by resetting the ambiguities of all tracked satellites, while other estimable parameters are kept in the Kalman filter with reserved covariances from the previous epoch. It can be seen that the initialization positioning errors of SDIC-RTPPP is slightly better than that of IF-RTPPP, while for the re-initialization positioning errors, the SDIC-RTPPP is much better than that of IF-RTPPP, which reflects the advantages of the proposed between-satellite SD ionospheric constraints on RTPPP in kinematic mode. After the convergence time of about 30 min, the positioning errors of SDIC-RTPPP and IF-RTPPP are almost the same and can be kept within several centimeters. Compared with the GPS-only RTPPP, the positioning performance of GPS + Galileo RTPPP can be improved, especially in the (re-)convergence time.

Figure 9 depicts the convergence time of kinematic DF-RTPPP with different solutions at 68% confidence level. In this assessment, we sort the absolute positioning errors of ten red stations at each epoch, and then the value lower than 68% of the absolute positioning errors at each epoch is collected during the first 1 h (Lou et al. 2016). As we can see, the initialization performance of SDIC-RTPPP is slight better than that of IF-RTPPP in the first 10 min, while after 10 min, two RTPPP models have similar performance. Regarding the GPS-only solution, the re-convergence positioning errors at the first epoch for SDIC-RTPPP, with an approximate 0.2 and 0.35 m in the horizontal and vertical components, respectively, present a distinct superiority IF-RTPPP, which is more than 0.6 m in all components. With the introduction of Galileo observations, the re-convergence positioning errors at the first epoch for GPS + Galileo SDIC-RTPPP can be reduced to 0.15 and 0.2 m in the horizontal and vertical components, respectively, which means that the proposed SDIC-RTPPP model can significantly improve the continuity and stability of real-time kinematic positioning in the case of re-initialization. In this research, the convergence time for the horizontal and vertical components is defined as when 68% of the positioning errors is lower than 0.1 m. The initialization time of GPS-only RTPPP is about 35 and 25 min at the horizontal and vertical components, respectively, whereas for GPS + Galileo RTPPP, this time can be reduced to 22 min in horizontal and 19 min in vertical. In the GPS + Galileo solutions, compared with the IF-RTPPP, the re-convergence time of SDIC-RTPPP can be reduced from 23 to 3 min in horizontal and from 10 to 9 min in vertical. Apparently, the re-convergence time of horizontal components in DF-RTPPP can be significantly shortened by introducing high-precision ionospheric constraints.

Table 2 summarizes the RMS of positioning errors of kinematic DF-RTPPP with different solutions for ten red stations during the test period from DoY 190–201 in 2020. Noted that the positioning errors after 3 h of convergence are used for statistics. It can be seen that SDIC-RTPPP and IF-RTPPP for GPS-only solutions show basically the same positioning accuracy in all three directions, which can be better than 1.5, 2.0 and 4.0 cm in the N, E and U components, respectively. Compared with GPS-only, the positioning accuracy of GPS + Galileo DF-RTPPP can be improved by 26.9 and 16.2% in the horizontal and vertical components, respectively.

Single-frequency RTPPP

Since the ionospheric delays can be eliminated in the GRAPHIC observations, the SF-RTPPP based on the GRAPHIC model is employed as the reference. In order to weaken the adverse effects of the code noises and multipath errors on the GRAPHIC-RTPPP, a real-time phase smoothing code method called the code noise and multipath correction (CNMC) filter was applied in this experiment (Chang et al. 2015). Figure 10 shows the kinematic positioning errors of SF-RTPPP with two models for different stations during the 3–24 h on DoY 190 in 2020. It is worth noting

Table 2 RMS of positioning errors of DF-RTPPP with different solutions in kinematic mode (unit: cm)

Solutions	*N*	*E*	*U*	2*D*	3*D*
IF-G	1.3	2.0	3.8	2.5	4.4
SDIC-G	1.3	2.1	3.7	2.6	4.4
IF-GE	1.1	1.5	3.3	1.9	3.7
SDIC-GE	1.1	1.5	3.1	1.9	3.6

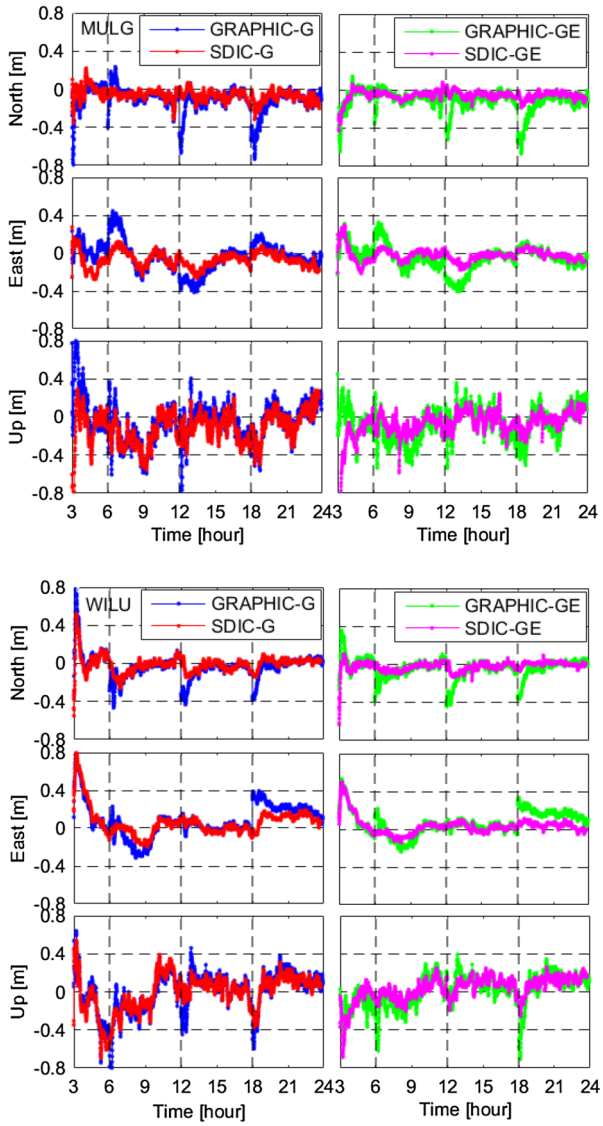

Fig.10 Kinematic positioning errors of single-frequency RTPPP with different solutions for MULG and WILU stations (DoY 190, 2020)

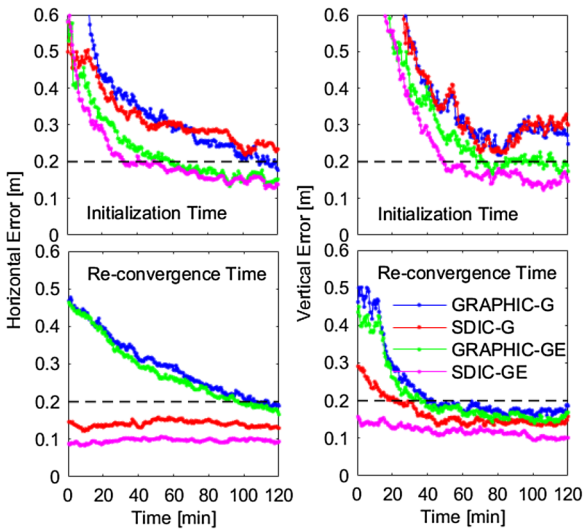

Fig.11 Convergence performance of kinematic single-frequency RTPPP with different solutions at the 68% confidence level (10 red stations, DoY 190–201, 2020)

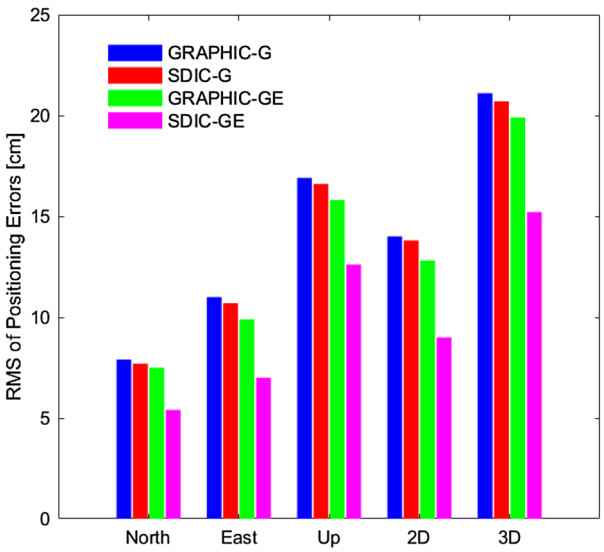

Fig. 12 RMS of kinematic positioning errors of SF-RTPPP with different solutions (ten red stations, DoY 190–201, 2020)

that the simulated signal interruptions are also introduced artificially at different times (GPST 06:00:00, 12:00:00 and 18:00:00). The initialization positioning errors of SDIC-RTPPP is lower than that of GRAPHIC-RTPPP, especially in the horizontal components. The time series of positioning errors for GRAPHIC-RTPPP after each interruption present apparent discontinuity, while for SDIC-RTPPP, the re-convergence positioning errors can be kept within 0.4 m. The main reason is that the SD ionospheric priori constraints can adequately compensate the ionospheric errors in the case of interruption. By introducing the Galileo observations, better positioning performance as expected can be achieved for both SDIC-RTPPP and GRAPHIC-RTPPP.

Figure 11 shows the convergence time of kinematic SF-RTPPP with different solutions at 68% confidence level. As we can see, the initialization performance of SDIC-RTPPP in the horizontal component during the first 60 min is better than that of GRAPHIC-RTPPP. Especially in the first 15 min, the horizontal errors of GPS SDIC-RTPPP can be lower than 0.5 m, while for GPS GRAPHIC-RTPPP, its errors exceed 0.8 m. With the introduction of Galileo observations, the initialization performance of GPS + Galileo SDIC-RTPPP, with an approximate 32 and 49 min for the horizontal and vertical errors to converge to 0.2 m, respectively, has a significant superiority over that of GPS + Galileo GRAPHIC-RTPPP, which is around 58 min in horizontal

and 72 min in vertical. As to GRAPHIC-RTPPP, 100 min in horizontal and 40 min in vertical need to be taken when re-converged to 0.2 m. While for SDIC-RTPPP, the horizontal re-convergence errors of GPS-only and GPS + Galileo can be maintained at 0.15 m and 0.1 m, respectively, the vertical re-convergence errors of GPS + Galileo solution can be kept within 0.15 m from the first epoch. Therefore, the problem of kinematic positioning discontinuities in the case of interruption could be well-solved by combining multi-GNSS observations and adding the proposed SD ionospheric constraints to RTPPP.

The RMS of positioning errors of kinematic SF-RTPPP with different solutions for ten red stations during the whole test period is shown in Fig. 12. We can see that the positioning accuracy of GPS-only SDIC-RTPPP and GPS-only GRAPHIC-RTPPP has similar performance and can be lower than 11.0 and 17.0 cm in the horizontal and vertical components, respectively. Different from the GPS-only solution, the positioning accuracy of GPS + Galileo SDIC-RTPPP, with RMS values of 9.0 and 12.6 cm in the horizontal and vertical components, respectively, is much better than that of GPS + Galileo GRAPHIC-RTPPP, which can be reached 12.8 cm in horizontal and 15.8 cm in vertical. Interestingly, it is found that the positioning accuracy of the SF-RTPPP based on the SD ionospheric constraints can be significantly improved after introducing the Galileo observations. Compared with GPS-only SDIC-RTPPP, the 3D positioning accuracy of GPS + Galileo SDIC-RTPPP can be improved by 26.6% to 15 cm.

Conclusions

The real-time and high-precision PPP with centimeter-level accuracy has become a mature positioning technology since the official service of IGS RTS in 2013. However, the (re-) convergence time of up to about 30 min restricts the possible positioning applications of kinematic RTPPP in complex environments. A new RTPPP model based on the regional between-satellite SD ionospheric constraints is proposed to achieve fast positioning in kinematic mode to reduce the initialization and re-convergence time.

Considering the adverse effect of time-varying receiver DCBs on ionospheric modeling, the between-satellite SD method is introduced into the regional ionospheric VTEC modeling. To obtain the high-precision line-of-sight ionospheric observables, the UU-PPP method rather than the traditional CCL method is employed to extract these observables. Since the huge computational burden coming with the estimation of ionospheric model coefficients will increase the complexity of server end and decrease the efficiency of user positioning in real-time, the polynomial function with simple structure and high efficiency is used for regional ionospheric modeling. The internal and external accord accuracy of the SD slant ionospheric delays retrieved from the regional between-satellite SD ionospheric VTEC model can be better than 2 and 8 cm, respectively. Besides, the dSTEC variations retrieved from three VTEC models are validated with the between-satellite SD and epoch-differenced GF combinations of dual-frequency phase observations, and the accuracy of the regional ionospheric model proposed in this contribution has priority over the CODE GIM and CNES real-time VTEC products.

In order to give full play to the advantages of the between-satellite SD ionospheric model, a new multi-GNSS RTPPP model based on the SD ionospheric constrained is proposed for the first time. After plenty of kinematic positioning tests, the new model's performance using SF and DF observations could be improved to some extent, especially in terms of (re-)convergence. As to GPS + Galileo DF solutions, the re-convergence errors of SDIC-RTPPP at the first epoch can be lower than 0.2 m in all directions, which is much better than that of IF-RTPPP with more than 0.6 m. Compared with the IF-RTPPP, the re-convergence time of SDIC-RTPPP when converged to 0.1 m at the 68% confidence level can be improved from 23 to 3 min and 10 to 9 min in the horizontal and vertical components, respectively. When it comes to GPS + Galileo SF solutions based on the GRAPHIC model, the initialization time of SDIC-RTPPP when converged to 0.2 m can be improved from 58 to 32 min in horizontal and 72 to 49 min in vertical, and positioning accuracy can be improved by 29.7 and 20.3% to 9.0 cm and 12.6 cm in the horizontal and vertical components, respectively. More importantly, the re-convergence errors of SF-SDIC-RTPPP in all directions from the first epoch can be maintained at about 0.15 m. Therefore, the proposed multi-GNSS SDIC-RTPPP model provides a good solution for the problem of kinematic positioning discontinuities when the satellite signals are blocked in a short time.

For higher performance and greater potential benefits of kinematic RTPPP in the future, the BDS-3 observations with three or more frequency signals could be added in the SDIC-RTPPP processing. Other widely used ionospheric modeling functions like spherical harmonic function can be applied to establish the regional between-satellite SD ionospheric VTEC model. Furthermore, the performance of the real-time between-satellite SD ionospheric model using multi-GNSS observations on ionospherically disturbed conditions or high solar activity need to be evaluated in future works.

Acknowledgements The authors would like to thank the GA (Geoscience Australia), CNES, GFZ and CODE for the provision of APREF observation data, real-time data streams including SSR satellite orbit and clock corrections as well as the VTEC products, final precise satellite orbits and clocks, post-processed DCB and final GIM products. Funded by State Key Laboratory of Geo-Information Engineering and Key Laboratory of Surveying and Mapping Science and Geospatial

Information Technology of MNR, CASM (No. 2021-01-08); the National Natural Science Foundation of China (No. 11673050); the Key R&D Program of Guangdong province (No. 2018B030325001).

Data availability The GNSS data are provided by the Asia–Pacific Reference Frame (APREF) network, which are available from ftp://ftp.ga.gov.au/geodesy-outgoing/gnss/data/. The merging broadcast ephemeris file (BRDM) is routinely generated as part of the Multi-GNSS Experiment (MGEX) at ftp://cddis.gsfc.nasa.gov/pub/gps/data/campaign/mgex/daily/rinex3/. The DCB and Center for Orbit Determination in Europe (CODE) GIM products are provided by the IGS analysis center at ftps://gdc.cddis.eosdis.nasa.gov/gnss/products/.

References

Ahmed F, Vaclavovic P, Teferle FN, Dousa J, Bingley R, Laurichesse D (2016) Comparative analysis of real-time precise point positioning zenith total delay estimates. GPS Solut 20:187–199

Caissy M, Agrotis L (2011) Real-time working group and real-time pilot project. Int GNSS Serv Tech Rep 2011:183–190

Chang Z, Hu X, Guo R, Cao Y, Wu X, Wang A, Dong E (2015) Comparison between CNMC and hatch filter & its precision analysis for BDS precise relative positioning (in Chinese). Sci Sin-Phys Mech Astron 45(7):079508

Chen L, Yi W, Song W, Shi C, Lou Y, Cao C (2018) Evaluation of three ionospheric delay computation methods for ground-based GNSS receivers. GPS Solut 22:125

Ciraolo L, Azpilicueta F, Brunini C, Meza A, Radicella SM (2007) Calibration errors on experimental slant total electron content (TEC) determined with GPS. J Geod 81:111–120

Feltens J, Angling M, Jackson-Booth N, Jakowski N, Hoque M, Hernandez-Pajares M, Aragon-Angel A, Orus R, Zandbergen R (2011) Comparative testing of four ionospheric models driven with GPS measurements. Radio Sci 46(6):1–11

Geng J, Bock Y (2016) GLONASS fractional-cycle bias estimation across inhomogeneous receivers for PPP ambiguity resolution. J Geod 90:379–396

Geng J, Meng X, Dodson AH, Ge M, Teferle FN (2010) Rapid re-convergences to ambiguity-fixed solutions in precise point positioning. J Geod 84:705–714

Guo F, Li X, Zhang X, Wang J (2017) The contribution of multi-GNSS experiment (MGEX) to precise point positioning. Adv Space Res 59:2714–2725

Hadas T, Bosy J (2015) IGS RTS precise orbits and clocks verification and quality degradation over time. GPS Solut 19(1):93–105

Hadas T, Kazmierski K, Sosnica K (2019) Performance of Galileo-only dual-frequency absolute positioning using the fully serviceable Galileo constellation. GPS Solut 23:108

Kazmierski K, Sosnica K, Hadas T (2018) Quality assessment of multi-GNSS orbits and clocks for real-time precise point positioning. GPS Solut 22:11

Kazmierski K, Zajdel R, Sosnica K (2020) Evolution of orbit and clock quality for real-time multi-GNSS solutions. GPS Solut 24:111

Kouba J, Heroux P (2001) Precise point positioning using IGS orbit and clock products. GPS Solut 5(2):12–28

Laurichesse D, Blot A (2016) Fast PPP convergence using multi-constellation and triple-frequency ambiguity resolution. In: Proceedings of ION GNSS+ 2016, Portland, Oregon, September 2016 pp. 2082–2088

Li X, Zhang X, Ge M (2011) Regional reference network augmented precise point positioning for instantaneous ambiguity resolution. J Geod 85:151–158

Li B, Zang N, Ge H, Shen Y (2019) Single-frequency PPP models: analytical and numerical comparison. J Geod 93:2499–2514

Li Z, Wang N, Hernandez-Pajares M, Yuan Y, Krankowski A, Liu A, Zha J, Garcia-Rigo A, Roma-Dollase D, Yang H, Laurichesse D, Blot A (2020) IGS real-time service for global ionospheric total electron content modeling. J Geod 94:32

Liu T, Yuan Y, Zhang B, Wang N, Tan B, Chen Y (2017) Multi-GNSS precise point positioning (MGPPP) using raw observations. J Geod 91:253–268

Liu T, Zhang B, Yuan Y, Li M (2018) Real-time precise point positioning (RTPPP) with raw observations and its application in real-time regional ionospheric VTEC modeling. J Geod 92(11):1267–1283

Liu T, Jiang W, Laurichesse D, Chen H, Liu X, Wang J (2020) Assessing GPS/Galileo real-time precise point positioning with ambiguity resolution based on phase biases from CNES. Adv Space Res 66(4):810–825

Lou Y, Zheng F, Gu S, Wang C, Guo H, Feng Y (2016) Multi-GNSS precise point positioning with raw single-frequency and dual-frequency measurement models. GPS Solut 20:849–862

Malys S, Jensen PA (1990) Geodetic point positioning with GPS carrier beat phase data from the CASA UNO experiment. Geophys Res Lett 17(5):651–654

Nie Z, Yang H, Zhou P, Gao Y, Wang Z (2019) Quality assessment of CNES real-time ionospheric products. GPS Solut 23:11

Petit G, Jiang Z (2008) Precise point positioning for TAI computation. Int J Navig Obs 2008:562878. https://doi.org/10.1155/2008/562878

Sanz J, Miguel Juan J, Rovira-Garcia A, Gonzalez-Casado G (2017) GPS differential code biases determination: methodology and analysis. GPS Solut 21(4):1549–1561

Schaer S (1999) Mapping and predicting the earth's ionosphere using the global positioning system. Ph.D. Dissertation, University of Berne, Switzerland

Shi C, Gu S, Lou Y, Ge M (2012) An improved approach to model ionospheric delays for single-frequency precise point positioning. Adv Space Res 49:1698–1708

Wang A, Chen J, Zhang Y, Meng L, Wang J (2019) Performance of selected ionospheric models in multi-global navigation satellite system single-frequency positioning over China. Remote Sens 11:2070

Wang A, Chen J, Zhang Y, Meng L, Wang B, Wang J (2020a) Evaluating the impact of CNES real-time ionospheric products on multi-GNSS single-frequency positioning using the IGS real-time service. Adv Space Res 66(11):2516–2527

Wang A, Chen J, Zhang Y, Wang J (2020b) Comparison of three widely used multi-GNSS real-time single-frequency precise point positioning models using the international GNSS service real-time service. IET Radar Sonar Navig 14:1726–1734

Wright TJ, Houlie N, Hildyard M, Iwabuchi T (2012) Real-time, reliable magnitudes for large earthquakes from 1 Hz GPS precise point positioning: the 2011 Tohoku-Oki (Japan) earthquake. Geophys Res Lett 39(12):L12302

Zhang B, Ou J, Yuan Y, Li Z (2012) Extraction of line-of-sight ionospheric observables from GPS data using precise point positioning. Sci China Earth Sci 55:1919–1928

Zhang Y, Chen J, Gong X, Chen Q (2020) The update of BDS-2 TGD and its impact on positioning. Adv Space Res 65(11):2645–2661

Zhou F, Dong D, Li P, Li X, Schuh H (2019) Influence of stochastic modeling for inter-system biases on multi-GNSS undifferenced and uncombined precise point positioning. GPS Solut 23:59

Zumberge JF, Heflin MB, Jefferson DC, Watkins MM, Webb FH (1997) Precise point positioning for the efficient and robust analysis of GPS data from large networks. J Geophys Res 102(B3):5005–5017

Ahao Wang is currently a lecturer at the College of Geoscience and Surveying Engineering, China University of Mining and Technology-Beijing, China. He received his PhD degree from Tongji University in 2021. His research mainly focuses on multi-GNSS PPP and its application in geoscience.

Yize Zhang is currently an associate professor at Shanghai Astronomical Observatory (SHAO). He received his PhD degree from Tongji University in 2017. Then, he did his postdoctoral researche at the Tokyo University of Marine Science and Technology (TUMSAT). His current research mainly focuses on multi-GNSS precise positioning and GNSS biases analysis.

Junping Chen is a professor and the head of the GNSS data analysis group at Shanghai Astronomical Observatory (SHAO). He received his PhD degree in Satellite Geodesy from Tongji University in 2007. Since 2011, he has been supported by the "one hundred talents" programs of the Chinese Academy of Sciences. His research interests include multi-GNSS data analysis and GNSS augmentation systems.

Hu Wang is currently an associate professor at the Chinese Academy of Surveying & Mapping. He received his PhD degree from Tongji University in 2012. His current research mainly focuses on GNSS PPP-AR and ionospheric modeling.